

Revisiting the impact of stellar magnetic activity on the detectability of solar-like oscillations by *Kepler*

Savita Mathur^{1,2,*}, Rafael A. García^{3,4}, Lisa Bugnet^{3,4}, Ângela R. G. Santos⁵,
Netsha Santiago⁶, and Paul G. Beck^{1,2,7}

¹*Instituto de Astrofísica de Canarias, La Laguna, Tenerife, Spain*

²*Dpto. de Astrofísica, Universidad de La Laguna, La Laguna, Tenerife, Spain*

³*IRFU, CEA, Université Paris-Saclay, Gif-sur-Yvette, France*

⁴*AIM, CEA, CNRS, Université Paris-Saclay, Université Paris Diderot, Sorbonne Paris Cité, F-91191 Gif-sur-Yvette, France*

⁵*Space Science Institute, 4750 Walnut Street, Suite 205, Boulder CO 80301, USA*

⁶*University of Puerto Rico at Cayey, Puerto Rico*

⁷*Department for Geophysics, Meteorology and Astrophysics, Institute of Physics, Karl-Franzens University of Graz, Universitätsplatz 5/II, 8010 Graz, Austria*

Correspondence*:
Savita Mathur
smathur@iac.es

ABSTRACT

Over 2,000 stars were observed for one month with a high enough cadence in order to look for acoustic modes during the survey phase of the *Kepler* mission. Solar-like oscillations have been detected in about 540 stars. The question of why no oscillations were detected in the remaining stars is still open. Previous works explained the non-detection of modes with the high level of magnetic activity of the stars. However, the sample of stars studied contained some classical pulsators and red giants that could have biased the results. In this work, we revisit this analysis on a cleaner sample of main-sequence solar-like stars that consists of 1,014 stars. First we compute the predicted amplitude of the modes of that sample and for the stars with detected oscillation and compare it to the noise at high frequency in the power spectrum. We find that the stars with detected modes have an amplitude to noise ratio larger than 0.94. We measure reliable rotation periods and the associated photometric magnetic index for 684 stars out of the full sample and in particular for 323 stars where the amplitude of the modes is predicted to be high enough to be detected. We find that among these 323 stars 32% of them have a level of magnetic activity larger than the Sun during its maximum activity, explaining the non-detection of acoustic modes. Interestingly, magnetic activity cannot be the primary reason responsible for the absence of detectable modes in the remaining 68% of the stars without acoustic modes detected and with reliable rotation periods. Thus, we investigate metallicity, inclination angle of the rotation axis, and binarity as possible causes of low mode amplitudes. Using spectroscopic observations for a subsample, we find that a low metallicity could be the reason for suppressed modes. No clear correlation with binarity nor inclination is found. We also derive the lower limit for our photometric activity index (of 20-30 ppm) below which rotation and magnetic activity are

not detected. Finally, with our analysis we conclude that stars with a photometric activity index larger than 2,000 ppm have 98.3% probability of not having oscillations detected.

Keywords: Asteroseismology, Stellar Rotation, Magnetic Activity, Main-sequence stars, Solar-like oscillations

1 INTRODUCTION

Solar-type stars show acoustic oscillations that are intrinsically damped and stochastically excited by near-surface convection [e.g. 32], which is also an important ingredient for magnetic activity [10, references therein].

In the Sun, the properties of the acoustic modes are sensitive to the varying magnetic activity [e.g. 72, 23, 35]. In particular, as a result of magnetic structures in the solar photosphere being strong absorbers of the acoustic waves [e.g. 8, 36], the amplitudes of the acoustic modes decrease with increasing activity level [e.g. 18, 41, 35, 38]. Already observed in the Sun, such activity-related variations were first discovered in a star other than the Sun, HD 49933 observed by the CoRoT satellite, by García et al. [30]. Searching for such signatures of magnetic activity in *Kepler* data, it was found that other solar-type stars, in particular KIC 8006161 and KIC 5184732, show evidence for a decrease in the mode heights with increasing activity [39, 63, 65].

The suppression of the acoustic modes by magnetic activity hampers their detection and, thus, magnetic activity may have important impact on the detectability of solar-type pulsators. In order to test this, Chaplin et al. [17] analyzed the first month of short-cadence *Kepler* data of about 2,000 stars. The authors successfully detected solar-type oscillations in only ~ 540 stars and found that as the activity level increases the number of detections decreases significantly. Thus, the non-detections were attributed to high activity levels. However, they were limited to one month of data, which on the one hand hampers the detection of acoustic oscillations and on the other hand, may bias the activity level estimates. Also, the sample of about 2,000 supposedly solar-like stars was polluted by other types of stars, in particular classical pulsators and red giants. Furthermore, since then, more accurate photometric proxies of magnetic activity have been developed. Indeed in the past several indexes were used mostly based on the standard deviation of the time series allowing to measure the variability of the stars. But this variability can be due to different phenomena such as oscillations, convection, or magnetic activity [e.g. 30, 2, 3, 17]. When measuring the magnetic activity index, we need to make sure that the variability is related to magnetic activity and not to other phenomena.

In this work, we analyze the latest data release of 2,576 targets observed in short-cadence by *Kepler*. Section 2 describes the data used and the selection of the sample. In Section 3, we describe the methods used to measure the surface rotation periods and the magnetic activity proxy. The surface rotation period is obtained by implementing the analysis in García et al. [27] and Ceillier et al. [16], which combines a time-frequency analysis with the auto-correlation function. Knowing the rotation period P_{rot} , we then measure the photometric magnetic activity index, which corresponds to the average value of the standard deviation of subseries of length $5 \times P_{\text{rot}}$ [S_{ph} ; e.g. 46]. Section 4 provides the results of this analysis. In Section 5, we study the impact of magnetic activity, metallicity, and stellar inclination on the detection of the acoustic modes, searching for correlations between those properties. Finally, Section 6 summarizes the main conclusions.

2 OBSERVATIONS: DEFINING THE SAMPLE

2.1 Data calibration

In this work, the *Kepler* light curves analyzed for rotation were generated from the long-cadence (29.4244 min) pixel files available at the Mikulski Archive for Space Telescopes (MAST) website. The integration of the stellar signal is done in masks larger than the usual ones used for exoplanet research in order to reduce the drifts induced by the displacement of the targets on the *Kepler* CCD. To do so, we take all the pixels centered at the coordinates of the star up to a radius for which a reference value per pixel, calculated as the 99.9 percentile of the weighted flux, is greater than 100. Then to correct for the remaining drifts, jumps and to stitch all the quarters together we follow the *Kepler* Asteroseismic Data Analysis and Calibration Software (KADACS)¹ methods described in García et al. [28]. The lightcurves produced in this way are low-pass filtered using three different cut-off periods at 20, 55, and 80 days. The filters are made in such a way that the transfer function is one up to the mentioned period and then it smoothly decrease to zero at the double period, ensuring some transmission of the signals until 40, 110 and 160 days respectively. Finally, gaps up to 20 days are interpolated using a multi-scale cosinus transform using inpainting techniques as described in García et al. [29] and Pires et al. [54]. As a comparison, we also use standard Pre-search Data Conditioning multi scale Maximum A-Posteriori light curves [PDC-msMAP, e.g., 69, 67, 70] to look for rotation periods and we compare the results with the three previously explained light curves. As shown in García et al. [26], it is more reliable to use different light curves prepared using completely different ways because each calibration system can fail for different reasons in particular targets. For the analysis of the rotation, we used all the quarters available in long cadence, i.e. 4 years of continuous data, except those quarters where the star falls on one of the bad modules of *Kepler*.

2.2 Target selection

The original sample was selected based on the target list of the Working Group 1 (WG1) of the *Kepler* Asteroseismic Science Consortium (KASC²) that focuses on solar-like stars. During the first 10 months of the mission, a survey phase was led in order to help the selection of the most promising targets for planet search or for asteroseismic analyses. As there were only 512 slots available to download the short-cadence data (due to the limited downlink bandwidth), each month a different sample of stars was targeted. Thus we start with a sample of 2,576 targets for which data was collected with a 58.85 s cadence.

First we remove four stars that do not have any effective temperature values. By studying the power spectrum, we can see that a fraction of these stars are classical pulsators or red giants. Classical pulsators usually present very high amplitude peaks in the power spectrum. We automatically discard stars which power spectra have peaks with amplitudes larger than $10^7 \text{ppm}^2 \mu\text{Hz}^{-1}$. As some of the remaining stars have an effective temperatures larger than 7,500K, we visually check them and find that they indeed have classical-pulsators like peaks. Since the amplitudes of these peaks are below our threshold they were not flagged by our automatic search.

The next step is to cross-check our sample with the legacy catalog of the *Kepler* red giants (García et al. in prep.). This catalog makes use of known red giants from the literature [e.g. 68, 48, 73]. In particular it also uses new techniques to classify the stars such as the FliPer method [11] or neural networks [34] as well as a visual inspection of all the stars. This leads to a sample of about 1,900 stars that should most probably be on the main sequence based on the lightcurves. Some of these stars that we discarded are not necessarily

¹ time-series are available at MAST via <https://doi.org/10.17909/t9-cfke-ps60>.

² <http://kasoc.phys.au.dk/>

misclassified but could be the result of some pollution as we use larger aperture than the ones optimized for planetary research. As we want to measure the rotation and level of magnetic activity of the stars, we prefer to remove any star whose lightcurve has some pollution to be sure that our study is not biased.

In this work we are interested in studying solar-like stars for which acoustic modes have not been detected. Thus we removed from the sample the solar-like stars that have detection of acoustic modes from Chaplin et al. [20], leading to a sample of 1,380 stars. In addition, we re-analyzed the latest data release (DR25) with the best calibration available. Indeed, the latest lightcurves processed by the *Kepler* Science office corrected some smearing effect that non-negligibly improved the noise at high-frequency leading to a higher signal-to-noise ratio and allowing us to detect acoustic (p) modes in additional stars. In order to search for acoustic modes in main-sequence stars, we use short-cadence data. Given that none of these 1,380 stars had oscillations detected, they were dropped off the short-cadence program to give priority to other targets and only have short-cadence data available for one month. We performed an asteroseismic analysis with the A2Z pipeline [49] and the FliPer [11] to look for signature of p modes. We confirmed the detection of oscillations in 42 stars and still have 92 candidates. The detailed analysis of these new detections will be presented in Mathur et al. (in prep.).

Finally, we also ran the FliPer_{Class} tool for classification [12] and did additional visual checks of the lightcurves. We found a sample of stars that presented peaks that did not look like the normal rotation behaviour we usually find so we decided to remove them from the sample.

After removing these stars, we end up with 1,014 stars that are supposed to be main-sequence stars and that do not show any signature of oscillations. Figure 1 represents the Hertzsprung-Russel (HR) Diagram where the effective temperature and the surface gravity come from the DR 25 *Kepler* stellar properties catalog [50]. The grey symbols represent the KASC WG1 stars observed in short cadence during the survey phase. The stars without oscillations detected are represented by black circles. We superimposed the stars with p-mode detections (red circles) and the new detection candidates (blue crosses). We will focus on the stars without detection of oscillations (or the non-oscillating stars) in the following sections. We also represent the HR Diagram of each sample in different panels for a better clarity.

2.3 Predicted mode amplitude

There is a clear relation between the amplitude of the modes and the luminosity of the stars. Kjeldsen and Bedding [40] and Brown [9] derived scaling relations based on the Sun that related the maximum amplitude of the solar-like oscillations and the stellar parameters. These relations have been used in particular to predict the amplitude of the modes for a given solar-like star [19, 14]. We used the relation of [14] where we removed the multiplicative factor of 0.85 that was taking into account the redder response of TESS compared to *Kepler*, leading to lower amplitudes. We computed the predicted maximum amplitude of the modes for the 1,014 stars without detection of acoustic modes and for the 529 stars with detected oscillations using the following relation:

$$A_{\max} = A_{\max,\odot} \times \beta \left(\frac{R}{R_{\odot}} \right)^2 \left(\frac{T_{\text{eff}}}{T_{\text{eff},\odot}} \right)^{0.5} \text{ ppm}, \quad (1)$$

where T_{eff} is the effective temperature, R is the stellar radius, and \odot denotes the solar values ($T_{\text{eff},\odot} = 5777 \text{ K}$; $R_{\odot} = 6.955 \times 10^{10} \text{ cm}$). $A_{\max,\odot}$ is the root-mean-square maximum amplitude for the Sun ($A_{\max,\odot} = 2.5 \text{ ppm}$). The factor β is a correction that depends on the temperature of the star and is defined as:

$$\beta = 1 - \exp\left(-\frac{T_{\text{red}} - T_{\text{eff}}}{1550}\right) \quad (2)$$

with $T_{\text{red}} = 8907(L/L_{\odot})^{-0.093}$ K.

Here, we used the temperatures from the DR25 *Kepler* star properties catalog [50] and radii from Berger et al. [6] that incorporated DR1 *Gaia* parallaxes to the previous catalog. We then computed the noise level for each star by taking the mean value of the power spectrum density in the frequency range 5,000 μHz to the Nyquist frequency for the short cadence (~ 8300 μHz). Figure 2 represents the ratio of the predicted amplitude and the high-frequency noise as a function of the effective temperature (top panel) and as a function of the surface gravity (bottom panel). As expected, we can see that a large fraction of the stars with detected oscillations (red symbols) have a ratio larger than 1. However 9 stars, which are on the main sequence, are just below. We checked the metallicity of those stars and there is no systematic behaviour. We also compared the predicted amplitudes with the observed amplitudes for that sample of stars. We found that in average, the predicted amplitudes are slightly overestimated compared to the observed ones. However, two of the most studied stars (KIC 8006161 and KIC 10644253) are predicted to have a ratio close to 1 but their observed signal-to-noise ratio (SNR) is much higher.

Given that around 280 non-oscillating stars have a predicted maximum amplitude lower than the high-frequency noise in the power spectrum, the non detection of the modes for that sample can be explained by the too low signal-to-noise ratio. For the remaining 734 stars with $A_{\text{max,pred}}/\text{Noise} \geq 1$, we should have detected the acoustic modes. As mentioned above, some stars with $A_{\text{max,pred}}/\text{Noise}$ slightly below 1 have modes detected so for the next sections, we will look into stars that follow the criteria:

$$\frac{A_{\text{max,pred}}}{\text{Noise}} > 0.94. \quad (3)$$

In addition, for the comparison with the stars where we detected modes, we select stars that are in the same region of the HR Diagram with:

$$T_{\text{eff}} \leq 6,800 \text{ K}, \quad (4)$$

and

$$\log g \leq 4.3 \text{ dex} \quad (5)$$

This yields a sample of 470 non-oscillating stars and 397 oscillating stars that are represented in Figure 3.

3 DATA ANALYSIS

In this section, we present the methodology used to measure the surface rotation of the stars and how we determine the level of magnetic activity using the photometric data of *Kepler*.

3.1 Measuring rotation period

The surface rotation period can be measured from photometric observations through the signature of the regular passage of spots inducing periodic modulations of the luminosity. Several methods were thus developed providing the measurements of the rotation of thousands of main-sequence stars observed by *Kepler* [e.g. 58, 27, 52]. These methods are based either on Lomb-Scargle periodograms [53], auto-correlation functions [ACF, 52], or wavelet-based analysis [71, 49]. In a blind hare-and-hounds exercise performed by most of the principal teams working on this topic with the *Kepler* data, Aigrain et al. [1] showed that the best combination of completeness and reliability was obtained with the analysis technique developed by García et al. [27] and Ceillier et al. [15] using a combination of period-search methods such as ACF and wavelets. In this work, we thus applied the pipeline from García et al. [27] to extract the surface rotation period of the 1,014 stars. We analyzed the three datasets corresponding to the three filters as described in Section 2.1. First we selected the stars where all the methods and all the filters agreed within 2σ , where $\sigma = \sqrt{\sigma_1^2 + \sigma_2^2}$ with σ_i being the uncertainty obtained by each method (except the ACF for which we do not compute any error). We also applied the criteria on the height of the ACF and the Composite Spectrum as described in Ceillier et al. [15]. We then visually checked the remaining stars that were not selected according to all these criteria.

We also analyzed the PDC-msMAP lightcurves to check for pollution as we use customized apertures with KADACS, which are more likely to be polluted. The crowding (that is the percentage of flux coming from the targeted star) of the stars in our sample is above 80%, i.e. they should have very little polluted light. However, one thing to keep in mind when studying the surface rotation periods of the stars is that the PDC-msMAP lightcurves can be filtered with a 21-day filter, which means that we can only detect rotation shorter than ~ 20 days [see the discussion in 26]. This also implies that for a star rotating slower, the PDC-msMAP analysis can lead to the detection of a harmonic. When the rotation period found with PDC-msMAP and KADACS agree within 2σ , we keep the rotation period found with the KADACS lightcurve. When the rotation obtained with PDC-msMAP is a harmonic of the period from KADACS, we also keep the rotation period from KADACS. Finally, if the rotation period (or a harmonic) is not found in the PDC-msMAP lightcurves, either the signal has been filtered out in these time series or the signal detected in the KADACS lightcurves could originate from a polluting star. Therefore, we discard this star.

3.2 Photometric activity level: S_{ph}

García et al. [30] showed in the case of the F-star HD 49933 observed by CoRoT that the variability of the lightcurve, estimated from the standard deviation of the observations, is associated to the existence of spots rotating on the surface of the star, and thus can be used as proxy of stellar activity. Since then, several metrics were developed and applied to study the stellar activity of the *Kepler* targets [2, 17, 51, 13]. However, the variability in the lightcurves can have different origins with different time scales such as magnetic activity but also convective motions, oscillations, or stellar companions. By taking into account the rotation of the star in its computation as it is done in Mathur et al. [51], the derived activity metric, so-called S_{ph} , is thus an actual proxy for magnetic variability. We first compute the standard deviation of subseries of length $5 \times P_{\text{rot}}$ [51]. Then we calculate the average of these standard deviations to derive the final $\langle S_{\text{ph}} \rangle$.

By comparing the $\langle S_{\text{ph}} \rangle$ with other classical proxies for the solar magnetic activity, such as sunspots or Ca II K-line emission, Salabert et al. [61] found a high correlation between the different magnetic proxies, showing the validity of our photometric proxy. Nevertheless, in the stellar case, the estimated proxy, S_{ph} , will depend on the inclination angle of the star in respect to the line of sight, on the moment

of the magnetic cycle when the star is observed, and the position of the active latitudes. These are also parameters that affect the spectroscopic observations for other classical proxies of stellar magnetic activity. So the S_{ph} is as good as a proxy as the Mount Wilson S-index. We just note that given the limitations listed above, it should be considered as a lower limit of the stellar photospheric activity.

4 RESULTS OF THE ANALYSIS

We performed the analysis of the rotation as described in the previous section for the full sample of 1,014 stars. The comparison of the different filters provided a list of reliable rotation periods for 412 stars. We then checked the remaining stars visually adding 278 stars to the sample. We decided to use the following priority for the values of the rotation period. First, we select the value from the wavelet analysis (when the values agree within 2σ), then we select the value from the composite spectrum, and finally the one computed with the ACF. The $\langle S_{\text{ph}} \rangle$ is the one computed with the finally selected rotation period. The analysis of the PDC lightcurves and the comparison of their results with the KADACS results flagged 38 stars that we checked visually. We found that 6 could be due to pollution and discarded them. We end up with a list of 684 stars with rotation periods measured. Table 1 provides the list of stars with their measured rotation periods, S_{ph} values, and their fundamental stellar parameters (effective temperature, surface gravity, and metallicity). Table 2 gives the list of stars without detection of rotation periods.

We classified the stars in a similar way to García et al. [27]: hot stars with $T_{\text{eff}} \geq 6250$ K, dwarfs with $T_{\text{eff}} < 6250$ K and $\log g > 4$ dex, and subgiants with $T_{\text{eff}} \leq 6250$ K and $\log g \leq 4.0$ dex. There are 313 stars from the studied sample coded as hot stars, 327 stars as dwarfs, and 44 stars as subgiants. They are showed in a HR Diagram in the left panel of Figure 4 where we color-coded the different spectral types defined above. The right panel shows the same diagram for the stars selected following criteria (3), (4), and (5).

Figure 5 represents the distribution of the rotation periods measured for the different categories of stars mentioned above, as well as for the full sample of stars with reliable measurements (black line). The left panel shows the hot stars and we clearly see that they are mostly rapid rotators as seen in García et al. [27]. This is in agreement with the theory as hot stars (i.e massive stars) have thinner outer convection zones leading to a smaller braking due to stellar winds. The mass limit between the hot stars and the cool stars is set to $1.3 M_{\odot}$ that is also called the Kraft break [42]. So around the subgiant phase, stars with higher masses than $1.3 M_{\odot}$ will not undergo braking while cooler stars with lower masses will slow down. However in the middle panel of Figure 5, we observe many dwarfs with small rotation periods. One explanation is that the fundamental stellar parameters (temperature and gravity) are less reliable and some stars in the dwarf sample might actually be hotter stars. Another plausible explanation is that these fast rotating cool stars are younger and have not yet slowed down. Comparing the rotation period of the subgiants (right panel of Figure 5) to the ones from the hot stars and the dwarfs, we find that the number of subgiants is much smaller. Indeed, stellar evolution theory predicts that when a star evolves on the subgiant branch, it slows down and its magnetic activity decreases, i.e. less spots are present at their surfaces. Since our measurements depend on the passage of spots on the stellar surfaces, we do not expect to measure the surface rotation in many of these more evolved stars. Our results corroborate this theory. We also notice that the subgiants with a measured rotation period are rather fast rotators (shorter than 30 days).

In Figure 6, we can see a histogram representation of the photospheric magnetic proxy, $\langle S_{\text{ph}} \rangle$, where the black dashed lines represent the range of the magnetic index of the Sun between minimum and maximum activity ($\langle S_{\text{ph},\odot,\text{min}} \rangle = 67.4$ ppm and $\langle S_{\text{ph},\odot,\text{max}} \rangle = 314.5$ ppm respectively). The hot

stars (left panel of Figure 6) have in general a similar level of magnetic activity to the Sun, while the dwarfs appear to be more active (middle panel of Figure 6), which is not what we expected. For these two categories, we see that the distribution peaks very close to the maximum activity of the Sun. Given the uncertainties on the magnetic index, we could say that stars where no acoustic modes have been detected have slightly larger magnetic activity levels than the Sun. As the sample of subgiants is very small we cannot conclude on their magnetic activity. Here again, this can be explained by the fact that subgiants are less active than main-sequence stars.

We then represent the distribution of the rotation periods (Figure 7) and the magnetic activity proxy (Figure 8) for the 323 non-oscillating stars as selected in Section 2.3 (criteria (3), (4), and (5)). We compare those distributions with the ones for the oscillating stars in the same region of the HR Diagram. For the hot stars (left panels), the distribution of the oscillating and non-oscillating stars are very similar, peaking at a rotation period below 5 days and at an $\langle S_{\text{ph}} \rangle$ value of 300 ppm. However, we can note that there are more non-oscillating stars with $\langle S_{\text{ph}} \rangle$ larger than 300 ppm. For the cool stars (middle panels), the rotation distributions are similar though there seems to be a bimodality. Given the small number of stars, it is not clear whether it is just a selection effect. Concerning the magnetic activity of the cool dwarfs, non-oscillating stars are more active than the oscillating ones. Finally for the subgiants, given the small number of non-oscillating subgiants, it is harder to compare the distributions. The rotation periods of the non-oscillating stars are in general shorter and somewhat more active compared to the oscillating ones, which could suggest that these are young subgiants.

5 DISCUSSION

In Figure 9, we show the magnetic index, S_{ph} , as a function of the rotation period, P_{rot} . We compare the non-oscillating stars studied in this work (black symbols) and the 310 oscillating stars with measured rotation periods from García et al. [27] (red symbols). The dashed lines delimit the region of minimum and maximum levels of magnetic activity of the Sun based on the VIRGO [Variability of solar IRradiance and Gravity Oscillations 24] photometric observations [27]. Figure 10 is the same as Figure 9 but for the stars with $A_{\text{max,pred}}/\text{Noise} > 0.94$ and selected in the same region of the HR Diagram.

5.1 Magnetic activity effect

We first start the analysis of the full sample. We can first notice that 252 stars ($\sim 80\%$) with detected oscillations have an $\langle S_{\text{ph}} \rangle$ value that falls in the same range as the Sun between minimum and maximum activity. Indeed, we expected that cool dwarfs with similar level of activity to the Sun have detection of p modes. However, we have 41 stars with a level of magnetic activity above the maximum of the Sun for which we have detected oscillations. We were not expecting them to have detected modes as they have high magnetic activity levels. We checked the maximum amplitude of the modes obtained from A2Z but those stars do not have a systematic low amplitude. They could be either subgiants or metal-rich stars [64, 45] enhancing the mode amplitudes and compensating the magnetic effect.

According to the DR25, 22 of these stars are subgiants so this could be a valid explanation for detecting their p modes (their intrinsic oscillations amplitudes are higher than during the main sequence). For the remaining 19 stars, the metallicity ($[\text{Fe}/\text{H}]$) obtained by the *Kepler* Follow-up Observations Program [25] also used in the DR25 stellar properties is super-solar for 12 stars. We still have 7 stars that have a high S_{ph} value, low $[\text{Fe}/\text{H}]$ but for which we could detect solar-like oscillations. This sounds reasonable given that for the Sun the amplitudes decrease by only around 12.5% [e.g. 38] so the amplitudes could still be large enough to be detected even for stars with a $\langle S_{\text{ph}} \rangle$ value above $\langle S_{\text{ph},\odot,\text{max}} \rangle$.

We see that below the S_{ph} at minimum solar activity, there are around 100 stars with rotation and magnetic activity detection whether they have detected p modes or not. We can consider that the threshold of rotation and magnetic activity detectability is $\sim 20\text{-}30$ ppm. We can also derive a threshold on $\langle S_{\text{ph}} \rangle$ of 2,000 ppm above which the probability of non detection of p modes is of 98.3%.

Regarding the stars without oscillations detected, as expected they have larger magnetic indexes compared to the oscillating sample. We find that 47.7% of the non-oscillating stars have an $\langle S_{\text{ph}} \rangle$ larger than $\langle S_{\text{ph},\odot,\text{max}} \rangle$. These stars agree and confirm that a high level of magnetic activity suppress the oscillations and can prevent us from detecting solar-like oscillations as also shown by Chaplin et al. [17].

If we now look at the 323 stars selected as described in Section 2.3 with a measured rotation period, we find that 103 stars have $\langle S_{\text{ph}} \rangle > \langle S_{\text{ph},\odot,\text{max}} \rangle$. So 68% of the stars where we expect high enough amplitudes to detect the acoustic modes have a level of activity similar to the Sun or lower. This is quite interesting and unexpected given the claim of Chaplin et al. [17] and the anti-correlation found between the Mount Wilson S-index and maximum amplitude of the modes for a small sample of stars by Bonanno et al. [7].

In Figure 11 and 12, we have divided the sample in the three categories for the full sample of stars and for the selected sample from criteria (3), (4), and (5) respectively in order to see where the different stars are situated in the HR Diagram. We can see that the non-oscillating hot stars (top left panels) are mostly concentrated in the same region as the oscillating stars. The cut from Section 2.3 removes some of the very active stars. The sample of cool dwarfs (top right panels) without detection of p modes contains many more active stars compared to the cool dwarfs with detected oscillations. The cut of the sample removes many of the high $\langle S_{\text{ph}} \rangle$ stars as many were very cool dwarfs with low expected amplitudes of the modes but some stars with high activity still remain. Finally the cut of the subgiants (bottom panels) removes some very active subgiants as well.

Since we find a large number of stars without detection of p modes and with magnetic indexes in the same range as the oscillating stars, we propose to investigate three explanations for these stars:

- the inclination angle affects the measurement of $\langle S_{\text{ph}} \rangle$ as with a low inclination angle not all the active regions are observed. As a consequence, the value we measure is just a lower limit of the real magnetic activity proxy of the star;
- correlation between the acoustic-mode amplitudes and the metallicity. Indeed it has been shown that metal poor stars have lower mode amplitudes [64, 47]. However metallicity also has an effect on the magnetic activity. Karoff et al. [37] showed how the magnetic activity level (obtained through the S-index and $\langle S_{\text{ph}} \rangle$) is larger for a super-metallic solar-like star. So the abundance can have two different effects that could also counter balance each other;
- the stars could be in a binary system [66]. Indeed a close-in companion could suppress p modes through tidal effects as it has been observed in red giants belonging to binary systems [31].

In Figure 13, we also represented the S_{ph} as a function of effective temperature. We do not see any correlation between the magnetic activity level and the T_{eff} . From Figure 1, the non-oscillating stars had a temperature range between 3,800 K and 7,500 K. We note that stars with very low levels of magnetic activity are rather hot stars with temperatures above 6,000 K.

5.2 Metallicity effect

Many of the non-oscillating stars have spectroscopic data obtained with the DR14 Apache Point Observatory Galactic Evolution Experiment survey [APOGEE 44, 33] and the DR2 Large Sky Area Multi-Object Fiber Spectroscopic Telescope survey [LAMOST 21, 43], providing metallicity values more precise than photometric observations. After cross-checking our sample of stars with $A_{\max, \text{pred}} > 0.94$ with the sample of these surveys we find that 158 stars have high-resolution spectroscopic observations from APOGEE and 326 stars have low-resolution spectroscopic data from LAMOST. We note that there could be an overlap between these two samples. Figure 14 shows the [Fe/H] histograms for APOGEE (top panel) and for LAMOST (lower panel) for all the non-oscillating stars that have a rotation and metallicity measurement (black solid line). We can see some differences between the two surveys, where it seems that the stars with APOGEE metallicity have an average of 0.05 dex while the ones with LAMOST observations have an average metallicity around -0.03 dex. We compared the metallicity from both surveys for a common sample of around 6,000 stars and found a trend where at low APOGEE [Fe/H], the LAMOST values are larger while at high APOGEE [Fe/H], the LAMOST values are smaller. We then did the comparison for the common sample of non-oscillating stars and in general LAMOST has lower [Fe/H] values compared to APOGEE, which can explain the difference in the histograms from the two surveys. Given that the usual spectroscopic uncertainties for metallicity is around 0.15 dex, we can still say that the two surveys are in agreement.

We then focus on the least active stars (with S_{ph} smaller than the maximum activity value for the Sun) that are represented with the blue dot-dash line while the stars more active are represented with a red line. In the LAMOST sample, we clearly see that the average metallicity of the stars is close to the solar one while the non-oscillating not too active stars have in general a sub-solar metallicity. We count 106 sub-solar metallic stars and 64 super-solar metallic stars. This agrees with the theory of Samadi et al. [64] a lower metallicity will lead to a less opaque convection zone and hence less energy for the excitation of the modes. As a consequence metal-poor stars are expected to have smaller acoustic-mode amplitudes.

However for the stars with APOGEE metallicity, it seems that the very active stars have both super and sub-solar metallicity. We find that 24 stars have sub-solar metallicity while 52 have super-solar metallicity. So the low metallicity only confirms the non detection of the modes in a smaller sample of stars. As mentioned earlier, high metallicity could also lead to a higher level of magnetic activity [37], which could explain the non-detection of the modes for some of the super-metallic stars. This competing effect could be the source of the unclear influence of the metallicity and its study is out of the scope of this work.

From this analysis, we note that the two surveys do not agree on the influence of metallicity. However as mentioned above within the typical uncertainties on [Fe/H] from spectroscopic observations, there is still some agreement. Besides the sample of stars being quite small the conclusions need to be taken cautiously. More high-resolution spectroscopic observations would be needed to better study that effect.

5.3 Inclination angle effect

The APOGEE spectroscopic observations also provide a measurement of the $v \sin i$ for some of our non-oscillating stars. By combining these values with the surface rotation periods measured with the *Kepler* data and with estimates of the radii from the DR25 stellar properties, we can estimate the inclination angles of a subsample of 162 stars selected to follow criteria (3). We obtain a reliable inclination angle, i , for 90 stars. For the other stars, the $\sin i$ is larger than 1. This could be due to a non-agreement between the rotation period and the $v \sin i$ or a less reliable radius, as the radii of these stars were mostly derived from isochrone fittings, hence less precise than asteroseismology. The typical uncertainties of the inclination

angles are around 25 degrees. Figure 15 represents the distribution of the inclination angles for those stars. We can see that they peak around an angle of 45 deg. We then study the sample of stars with an $\langle S_{\text{ph}} \rangle$ lower than $\langle S_{\text{ph},\odot,\text{max}} \rangle$ as we want to understand why the modes of these stars are not detected. The distribution (dashed red line in Figure 15) is slightly flatter but the median value is still around 45 deg. Since some of these stars also have a low metallicity that already explains the non-detection of the modes, we selected the stars with a metallicity larger than the Sun. That sample consists of 13 stars, among which 4 stars have a low inclination angle and 9 have an inclination angle above 45 deg (blue dot-dash line). With this small number of stars, we cannot conclude that the low-inclination is responsible for the low $\langle S_{\text{ph}} \rangle$.

5.4 Binarity effect

We cross-checked our sample of stars with the stars flagged as binary with the *Gaia* catalog [6]. Among our sample of non-oscillating stars with rotation periods, 614 stars are included in the aforementioned catalog. We found that 8 stars of our sample are potential binaries. KIC 4057892, KIC 4930560, KIC 8737920, and KIC 12470631 have a flag 1 standing for a binary candidate based on the Gaia radius. KIC 4276716, KIC 5564082, KIC 5617510, and KIC 8396660 have a flag 2, meaning that they are AO-detected binaries [74].

Recently, Schonhut-Stasik et al. [66] studied how a stellar companion can suppress acoustic modes. They obtained ROBO-AO images and/or RV measurements for a sample of 327 stars (including red giants and solar-like stars without detection of modes and with low-amplitude modes). No clear difference between oscillating stars and non-oscillating stars was found, whether in terms of close or wide binarity. They conclude that binarity is not the only mechanism to inhibit oscillations.

We cross-checked our sample of stars with reliable rotation periods and photometric magnetic index with their binary stars and found only three stars in common. Two of them have an $\langle S_{\text{ph}} \rangle$ below $\langle S_{\text{ph},\odot,\text{max}} \rangle$. We would need a larger sample of stars with measured RV.

5.5 HERMES observations

Because non-oscillating stars are not typical targets of large-scale spectroscopic surveys, we started to pay close attention to those targets within our own spectroscopic observing programs. [4, 5] and [60, 62] performed spectroscopy of 18 oscillating solar analogues with the Hermes high-resolution spectrograph [56, 55], mounted on the 1.2 m Mercator telescope on La Palma, Canary Islands. We extended this program to cover a larger sample of oscillating as well as non-oscillating targets. Observing time was granted and will be executed in the coming semesters.

As a proof of concept we can discuss the first three non-oscillating stars for which we obtained spectroscopic observations, KIC 11498538, KIC 7841024, KIC 7898839. Note that the first of these stars (KIC 11498538) is not in our sample anymore as it was flagged by the *FliPer_{Class}* tool as a possible classical pulsator. According to the literature, that star is actually listed as an eruptive variable star, agreeing with the peculiar flag of *FliPer_{Class}*. However being included in the preliminary work and still a candidate of a fast rotator without detection of oscillations, we will discuss the spectroscopic analysis of that star. For the other two stars we have computed that the predicted amplitude of the modes is much larger than the noise.

All stars have a significantly higher chromospheric activity than the Sun. KIC 7898839 was chosen because of its solar-like rotation period of 28 days. For the two other stars, a rotation period of ~ 3 days was derived from *Kepler* photometry. Despite the similar rotation period KIC 11498538 shows signs of significantly broader rotational broadening than KIC 7841024, suggesting that the latter one is seen towards

a pole-on inclination. We refrain from comparing the stars on the basis of the Mount-Wilson S-index [22], as such large rotational velocities are likely to broaden the emission peak beyond the narrow wavelength range, defined by the triangular filters.

Currently, these are only first diagnostics from a small sample of stars. We plan to have a final sample of several dozens of stars, all obtained with the same spectrograph, which will then be consistently analyzed.

6 CONCLUSIONS

We have revisited the analysis of the 2,576 stars observed during the survey phase of main-sequence solar-like pulsating stars of the *Kepler* mission with one month of short-cadence data and followed for four years in long cadence. After removing polluting stars (red giants, classical pulsators, stars with already detected solar-like oscillations, new detection of solar-like oscillations, probable pollution), we have a sample of 1,014 main-sequence and subgiant solar-like stars. We measured the surface rotation period, P_{rot} , and the photometric magnetic activity index, $\langle S_{\text{ph}} \rangle$ and obtained reliable values for 684 stars, representing a yield of 67.4%. As expected the hot stars rotate in general faster than the cool dwarfs. Our sample of subgiants is too small to conclude anything about them.

- We have computed the predicted amplitude of the modes for the 1,014 stars of our sample and compared it to the high-frequency noise in the power spectrum. The majority of the stars with detected oscillations have a ratio between the predicted amplitude and the noise above 1, with only 16 stars below. We found that for 394 non-oscillating stars, that ratio is below 1.
- We can provide a lower limit of detection of magnetic activity of 20-30 ppm below which we do not detect any rotation periods.
- If we discard the stars for which the predicted amplitude of the modes is smaller than the noise, we find that only 32% (compared to 47.7% for the full sample) of the stars have a magnetic activity larger than the Sun at maximum activity. While magnetic activity explains the non detection of the modes for some stars, this is not the case for a large fraction of the stars without detection of oscillations.
- Based on our samples and the analysis presented here, we conclude that if a star has an $\langle S_{\text{ph}} \rangle$ larger than 2000 ppm, it has 98.7% probability that we will not detect oscillations.
- We notice a sample of stars with a high magnetic activity level and for which p modes have been detected. We found that 12 stars have a high [Fe/H] and 22 stars are subgiants, which could explain the enhancement of the modes in spite of their large $\langle S_{\text{ph}} \rangle$ values.
- The study of the remaining stars without detection of modes shows that low metallicity could be an explanation but given that high-resolution spectroscopic observations for those stars were available only for only 158 stars, we cannot firmly conclude.
- We also investigated the inclination angle using radius from the DR25 *Kepler* stellar properties catalog and $v \sin i$ from APOGEE but no clear correlation was found. However the $v \sin i$ was available for a small sample of stars and the radius from the isochrone fitting from DR25 are not the most precise values, which could bias our analysis.
- We checked whether the stars belonged to binary systems and only a handful of them are flagged as binaries either by *Gaia* or by AO observations.
- The preliminary analysis of the spectroscopic observations from the HERMES instrument for three stars shows that they have a high level of chromospheric activity.

While magnetic activity seems to explain the non-detection of oscillations in almost half of the sample and some hints that metallicity can also play a role, we still have stars for which there is no clear and firm explanation. We would need additional spectroscopic observations (that are underway).

Understanding the non-detection of oscillations is very important given the future missions like the NASA Transiting Exoplanet Survey Satellite [TESS, 59] already launched and the ESA PLANetary Transits and Oscillations of stars [PLATO, 57] coming up as they rely on the detection of solar-like oscillations to better characterize the stars, in particular the ones hosting planets.

REFERENCES

- [1] Aigrain, S., Llama, J., Ceillier, T., Chagas, M. L. d., Davenport, J. R. A., García, R. A., et al. (2015). Testing the recovery of stellar rotation signals from Kepler light curves using a blind hare-and-hounds exercise. *MNRAS* 450, 3211–3226. doi:10.1093/mnras/stv853
- [2] Basri, G., Walkowicz, L. M., Batalha, N., Gilliland, R. L., Jenkins, J., Borucki, W. J., et al. (2010). Photometric Variability in Kepler Target Stars: The Sun Among Stars—a First Look. *ApJL* 713, L155–L159. doi:10.1088/2041-8205/713/2/L155
- [3] Basri, G., Walkowicz, L. M., Batalha, N., Gilliland, R. L., Jenkins, J., Borucki, W. J., et al. (2011). Photometric Variability in Kepler Target Stars. II. An Overview of Amplitude, Periodicity, and Rotation in First Quarter Data. *AJ* 141, 20. doi:10.1088/0004-6256/141/1/20
- [4] Beck, P. G., Allende Prieto, C., Van Reeth, T., Tkachenko, A., Raskin, G., van Winckel, H., et al. (2016). The HERMES solar atlas and the spectroscopic analysis of the seismic solar analogue KIC 3241581. *A&A* 589, A27. doi:10.1051/0004-6361/201425423
- [5] Beck, P. G., do Nascimento, J.-D., Jr., Duarte, T., Salabert, D., Tkachenko, A., Mathis, S., et al. (2017). Lithium abundance and rotation of seismic solar analogues. Solar and stellar connection from Kepler and Hermes observations. *A&A* 602, A63. doi:10.1051/0004-6361/201629820
- [6] Berger, T. A., Huber, D., Gaidos, E., and van Saders, J. L. (2018). Revised Radii of Kepler Stars and Planets Using Gaia Data Release 2. *ApJ* 866, 99. doi:10.3847/1538-4357/aada83
- [7] Bonanno, A., Corsaro, E., and Karoff, C. (2014). Asteroseismic stellar activity relations. *A&A* 571, A35. doi:10.1051/0004-6361/201424632
- [8] Braun, D. C., Duvall, T. L., Jr., and Labonte, B. J. (1987). Acoustic absorption by sunspots. *ApJL* 319, L27–L31. doi:10.1086/184949
- [9] Brown, T. M. (1991). The source of solar high-frequency acoustic modes - Theoretical expectations. *ApJ* 371, 396–401. doi:10.1086/169900
- [10] Brun, A. S. and Browning, M. K. (2017). Magnetism, dynamo action and the solar-stellar connection. *Living Reviews in Solar Physics* 14, 4. doi:10.1007/s41116-017-0007-8
- [11] Bugnet, L., García, R. A., Davies, G. R., Mathur, S., Corsaro, E., Hall, O. J., et al. (2018). FliPer: A global measure of power density to estimate surface gravities of main-sequence solar-like stars and red giants. *A&A* 620, A38. doi:10.1051/0004-6361/201833106
- [12] Bugnet, L., García, R. A., Mathur, S., Davies, G. R., Hall, O. J., Lund, M. N., et al. (2019). FliPer_{Class}: In search of solar-like pulsators among TESS targets. *A&A* 624, A79. doi:10.1051/0004-6361/201834780
- [13] Campante, T. L., Chaplin, W. J., Lund, M. N., Huber, D., Hekker, S., García, R. A., et al. (2014). Limits on Surface Gravities of Kepler Planet-candidate Host Stars from Non-detection of Solar-like Oscillations. *ApJ* 783, 123. doi:10.1088/0004-637X/783/2/123

- [14] Campante, T. L., Schofield, M., Kuszlewicz, J. S., Bouma, L., Chaplin, W. J., Huber, D., et al. (2016). The Asteroseismic Potential of TESS: Exoplanet-host Stars. *ApJ* 830, 138. doi:10.3847/0004-637X/830/2/138
- [15] Ceillier, T., Tayar, J., Mathur, S., Salabert, D., García, R. A., Stello, D., et al. (2017). Surface rotation of Kepler red giant stars. *A&A* 605, A111. doi:10.1051/0004-6361/201629884
- [16] Ceillier, T., van Saders, J., García, R. A., Metcalfe, T. S., Creevey, O., Mathis, S., et al. (2016). Rotation periods and seismic ages of KOIs - comparison with stars without detected planets from Kepler observations. *MNRAS* 456, 119–125. doi:10.1093/mnras/stv2622
- [17] Chaplin, W. J., Bedding, T. R., Bonanno, A., Broomhall, A.-M., García, R. A., Hekker, S., et al. (2011). Evidence for the Impact of Stellar Activity on the Detectability of Solar-like Oscillations Observed by Kepler. *ApJL* 732, L5. doi:10.1088/2041-8205/732/1/L5
- [18] Chaplin, W. J., Elsworth, Y., Isaak, G. R., Miller, B. A., and New, R. (2000). Variations in the excitation and damping of low- l solar p modes over the solar activity cycle*. *MNRAS* 313, 32–42. doi:10.1046/j.1365-8711.2000.03176.x
- [19] Chaplin, W. J., Kjeldsen, H., Bedding, T. R., Christensen-Dalsgaard, J., Gilliland, R. L., Kawaler, S. D., et al. (2011). Predicting the Detectability of Oscillations in Solar-type Stars Observed by Kepler. *ApJ* 732, 54–+. doi:10.1088/0004-637X/732/1/54
- [20] Chaplin, W. J., Kjeldsen, H., Christensen-Dalsgaard, J., Basu, S., Miglio, A., Appourchaux, T., et al. (2011). Ensemble Asteroseismology of Solar-Type Stars with the NASA Kepler Mission. *Science* 332, 213–. doi:10.1126/science.1201827
- [21] De Cat, P., Fu, J. N., Ren, A. B., Yang, X. H., Shi, J. R., Luo, A. L., et al. (2015). Lamost Observations in the Kepler Field. I. Database of Low-resolution Spectra. *ApJS* 220, 19. doi:10.1088/0067-0049/220/1/19
- [22] Duncan, D. K., Vaughan, A. H., Wilson, O. C., Preston, G. W., Frazer, J., Lanning, H., et al. (1991). CA II H and K measurements made at Mount Wilson Observatory, 1966-1983. *ApJS* 76, 383–430. doi:10.1086/191572
- [23] Elsworth, Y., Howe, R., Isaak, G. R., McLeod, C. P., and New, R. (1990). Variation of low-order acoustic solar oscillations over the solar cycle. *Nature* 345, 322–324. doi:10.1038/345322a0
- [24] Fröhlich, C., Romero, J., Roth, H., Wehrli, C., Andersen, B. N., Appourchaux, T., et al. (1995). VIRGO: Experiment for Helioseismology and Solar Irradiance Monitoring. *Sol. Phys.* 162, 101–128. doi:10.1007/BF00733428
- [25] Furlan, E., Ciardi, D. R., Cochran, W. D., Everett, M. E., Latham, D. W., Marcy, G. W., et al. (2018). The Kepler Follow-up Observation Program. II. Stellar Parameters from Medium- and High-resolution Spectroscopy. *ApJ* 861, 149. doi:10.3847/1538-4357/aaca34
- [26] García, R. A., Ceillier, T., Mathur, S., and Salabert, D. (2013). Measuring Reliable Surface Rotation Rates from Kepler Photometric Observations. In *Astronomical Society of the Pacific Conference Series*, eds. H. Shibahashi and A. E. Lynas-Gray. vol. 479 of *Astronomical Society of the Pacific Conference Series*, 129
- [27] García, R. A., Ceillier, T., Salabert, D., Mathur, S., van Saders, J. L., Pinsonneault, M., et al. (2014). Rotation and magnetism of Kepler pulsating solar-like stars. Towards asteroseismically calibrated age-rotation relations. *A&A* 572, A34. doi:10.1051/0004-6361/201423888
- [28] García, R. A., Hekker, S., Stello, D., Gutiérrez-Soto, J., Handberg, R., Huber, D., et al. (2011). Preparation of Kepler light curves for asteroseismic analyses. *MNRAS* 414, L6–L10. doi:10.1111/j.1745-3933.2011.01042.x

- [29] García, R. A., Mathur, S., Pires, S., Régulo, C., Bellamy, B., Pallé, P. L., et al. (2014). Impact on asteroseismic analyses of regular gaps in Kepler data. *A&A* 568, A10. doi:10.1051/0004-6361/201323326
- [30] García, R. A., Mathur, S., Salabert, D., Ballot, J., Régulo, C., Metcalfe, T. S., et al. (2010). CoRoT Reveals a Magnetic Activity Cycle in a Sun-Like Star. *Science* 329, 1032–. doi:10.1126/science.1191064
- [31] Gaulme, P., Jackiewicz, J., Appourchaux, T., and Mosser, B. (2014). Surface Activity and Oscillation Amplitudes of Red Giants in Eclipsing Binaries. *ApJ* 785, 5. doi:10.1088/0004-637X/785/1/5
- [32] Goldreich, P. and Keeley, D. A. (1977). Solar seismology. II - The stochastic excitation of the solar p-modes by turbulent convection. *ApJ* 212, 243–251. doi:10.1086/155043
- [33] Holtzman, J. A., Hesselquist, S., Shetrone, M., Cunha, K., Allende Prieto, C., Anguiano, B., et al. (2018). APOGEE Data Releases 13 and 14: Data and Analysis. *AJ* 156, 125. doi:10.3847/1538-3881/aad4f9
- [34] Hon, M., Stello, D., and Yu, J. (2018). Deep learning classification in asteroseismology using an improved neural network: results on 15 000 Kepler red giants and applications to K2 and TESS data. *MNRAS* 476, 3233–3244. doi:10.1093/mnras/sty483
- [35] Howe, R., Davies, G. R., Chaplin, W. J., Elsworth, Y. P., and Hale, S. J. (2015). Validation of solar-cycle changes in low-degree helioseismic parameters from the Birmingham Solar-Oscillations Network. *MNRAS* 454, 4120–4141. doi:10.1093/mnras/stv2210
- [36] Jain, R. and Haber, D. (2002). Solar p-modes and surface magnetic fields: Is there an acoustic emission?. MDI/SOHO observations. *A&A* 387, 1092–1099. doi:10.1051/0004-6361:20020310
- [37] Karoff, C., Metcalfe, T. S., Santos, Â. R. G., Montet, B. T., Isaacson, H., Witzke, V., et al. (2018). The Influence of Metallicity on Stellar Differential Rotation and Magnetic Activity. *ApJ* 852, 46. doi:10.3847/1538-4357/aaa026
- [38] Kiefer, R., Komm, R., Hill, F., Broomhall, A.-M., and Roth, M. (2018). GONG p-Mode Parameters Through Two Solar Cycles. *Sol. Phys.* 293, 151. doi:10.1007/s11207-018-1370-x
- [39] Kiefer, R., Schad, A., Davies, G., and Roth, M. (2017). Stellar magnetic activity and variability of oscillation parameters: An investigation of 24 solar-like stars observed by Kepler. *A&A* 598, A77. doi:10.1051/0004-6361/201628469
- [40] Kjeldsen, H. and Bedding, T. R. (1995). Amplitudes of stellar oscillations: the implications for asteroseismology. *A&A* 293, 87–106
- [41] Komm, R. W., Howe, R., and Hill, F. (2000). Solar-Cycle Changes in Gong P-Mode Widths and Amplitudes 1995-1998. *ApJ* 531, 1094–1108. doi:10.1086/308518
- [42] Kraft, R. P. (1967). Studies of Stellar Rotation. V. The Dependence of Rotation on Age among Solar-Type Stars. *ApJ* 150, 551. doi:10.1086/149359
- [43] Luo, A.-L., Zhao, Y.-H., Zhao, G., Deng, L.-C., Liu, X.-W., Jing, Y.-P., et al. (2016). VizieR Online Data Catalog: LAMOST DR2 catalogs (Luo+, 2016). *VizieR Online Data Catalog* 5149
- [44] Majewski, S. R., Schiavon, R. P., Frinchaboy, P. M., Allende Prieto, C., Barkhouser, R., Bizyaev, D., et al. (2017). The Apache Point Observatory Galactic Evolution Experiment (APOGEE). *AJ* 154, 94. doi:10.3847/1538-3881/aa784d
- [45] Mathur, S., Bruntt, H., Catala, C., Benomar, O., Davies, G. R., García, R. A., et al. (2013). Study of HD 169392A observed by CoRoT and HARPS. *A&A* 549, A12. doi:10.1051/0004-6361/201219678
- [46] Mathur, S., García, R. A., Ballot, J., Ceillier, T., Salabert, D., Metcalfe, T. S., et al. (2014). Magnetic activity of F stars observed by Kepler. *A&A* 562, A124. doi:10.1051/0004-6361/201322707

- [47] Mathur, S., García, R. A., Catala, C., Bruntt, H., Mosser, B., Appourchaux, T., et al. (2010). The solar-like CoRoT target HD 170987: spectroscopic and seismic observations. *A&A* 518, A53. doi:10.1051/0004-6361/201014103
- [48] Mathur, S., García, R. A., Huber, D., Regulo, C., Stello, D., Beck, P. G., et al. (2016). Probing the Deep End of the Milky Way with Kepler: Asteroseismic Analysis of 854 Faint Red Giants Misclassified as Cool Dwarfs. *ApJ* 827, 50. doi:10.3847/0004-637X/827/1/50
- [49] Mathur, S., García, R. A., Régulo, C., Creevey, O. L., Ballot, J., Salabert, D., et al. (2010). Determining global parameters of the oscillations of solar-like stars. *A&A* 511, A46. doi:10.1051/0004-6361/200913266
- [50] Mathur, S., Huber, D., Batalha, N. M., Ciardi, D. R., Bastien, F. A., Bieryla, A., et al. (2017). Revised Stellar Properties of Kepler Targets for the Q1-17 (DR25) Transit Detection Run. *ApJS* 229, 30. doi:10.3847/1538-4365/229/2/30
- [51] Mathur, S., Salabert, D., García, R. A., and Ceillier, T. (2014). Photometric magnetic-activity metrics tested with the Sun: application to Kepler M dwarfs. *Journal of Space Weather and Space Climate* 4, A15. doi:10.1051/swsc/2014011
- [52] McQuillan, A., Mazeh, T., and Aigrain, S. (2014). Rotation Periods of 34,030 Kepler Main-sequence Stars: The Full Autocorrelation Sample. *ApJS* 211, 24. doi:10.1088/0067-0049/211/2/24
- [53] Nielsen, M. B., Gizon, L., Schunker, H., and Karoff, C. (2013). Rotation periods of 12 000 main-sequence Kepler stars: Dependence on stellar spectral type and comparison with $v \sin i$ observations. *A&A* 557, L10. doi:10.1051/0004-6361/201321912
- [54] Pires, S., Mathur, S., García, R. A., Ballot, J., Stello, D., and Sato, K. (2015). Gap interpolation by inpainting methods: Application to ground and space-based asteroseismic data. *A&A* 574, A18. doi:10.1051/0004-6361/201322361
- [55] Raskin, G. (2011). *Hermes, a fibre-fed high-resolution spectrograph for the Mercator Telescope*. Ph.D. thesis, Institute of Astronomy, Katholieke Universiteit Leuven, Belgium
- [56] Raskin, G., van Winckel, H., Hensberge, H., Jorissen, A., Lehmann, H., Waelkens, C., et al. (2011). HERMES: a high-resolution fibre-fed spectrograph for the Mercator telescope. *A&A* 526, A69. doi:10.1051/0004-6361/201015435
- [57] Rauer, H., Catala, C., Aerts, C., Appourchaux, T., Benz, W., Brandeker, A., et al. (2014). The PLATO 2.0 mission. *Experimental Astronomy* 38, 249–330. doi:10.1007/s10686-014-9383-4
- [58] Reinhold, T., Reiners, A., and Basri, G. (2013). Rotation and differential rotation of active Kepler stars. *A&A* 560, A4. doi:10.1051/0004-6361/201321970
- [59] Ricker, G. R., Winn, J. N., Vanderspek, R., Latham, D. W., Bakos, G. Á., Bean, J. L., et al. (2015). Transiting Exoplanet Survey Satellite (TESS). *Journal of Astronomical Telescopes, Instruments, and Systems* 1, 014003. doi:10.1117/1.JATIS.1.1.014003
- [60] Salabert, D., García, R. A., Beck, P. G., Egeland, R., Pallé, P. L., Mathur, S., et al. (2016). Photospheric and chromospheric magnetic activity of seismic solar analogs. Observational inputs on the solar-stellar connection from Kepler and Hermes. *A&A* 596, A31. doi:10.1051/0004-6361/201628583
- [61] Salabert, D., García, R. A., Jiménez, A., Bertello, L., Corsaro, E., and Pallé, P. L. (2017). Photospheric activity of the Sun with VIRGO and GOLF. Comparison with standard activity proxies. *A&A* 608, A87. doi:10.1051/0004-6361/201731560
- [62] Salabert, D., Régulo, C., García, R. A., Beck, P. G., Ballot, J., Creevey, O. L., et al. (2016). Magnetic variability in the young solar analog KIC 10644253. Observations from the Kepler satellite and the HERMES spectrograph. *A&A* 589, A118. doi:10.1051/0004-6361/201527978

- [63] Salabert, D., Régulo, C., Pérez Hernández, F., and García, R. A. (2018). Frequency dependence of p-mode frequency shifts induced by magnetic activity in Kepler solar-like stars. *A&A* 611, A84. doi:10.1051/0004-6361/201731714
- [64] Samadi, R., Ludwig, H.-G., Belkacem, K., Goupil, M. J., and Dupret, M.-A. (2010). The CoRoT target HD 49933 . I. Effect of the metal abundance on the mode excitation rates. *A&A* 509, A15. doi:10.1051/0004-6361/200911867
- [65] Santos, A. R. G., Campante, T. L., Chaplin, W. J., Cunha, M. S., Lund, M. N., Kiefer, R., et al. (2018). Signatures of Magnetic Activity in the Seismic Data of Solar-type Stars Observed by Kepler. *ApJS* 237, 17. doi:10.3847/1538-4365/aac9b6
- [66] Schonhut-Stasik, J., Huber, D., Baranec, C., Lamman, C., Salama, M., Jensen-Clem, R., et al. (2019). Robo-ao kepler asteroseismic survey. ii. do stellar companions inhibit stellar oscillations? *ApJ*, submitted
- [67] Smith, J. C., Stumpe, M. C., Van Cleve, J. E., Jenkins, J. M., Barclay, T. S., Fanelli, M. N., et al. (2012). Kepler Presearch Data Conditioning II - A Bayesian Approach to Systematic Error Correction. *PASP* 124, 1000–1014. doi:10.1086/667697
- [68] Stello, D., Huber, D., Bedding, T. R., Benomar, O., Bildsten, L., Elsworth, Y. P., et al. (2013). Asteroseismic Classification of Stellar Populations among 13,000 Red Giants Observed by Kepler. *ApJL* 765, L41. doi:10.1088/2041-8205/765/2/L41
- [69] Stumpe, M. C., Smith, J. C., Van Cleve, J. E., Twicken, J. D., Barclay, T. S., Fanelli, M. N., et al. (2012). Kepler Presearch Data Conditioning I - Architecture and Algorithms for Error Correction in Kepler Light Curves. *PASP* 124, 985–999. doi:10.1086/667698
- [70] Thompson, S. E., Christiansen, J. L., Jenkins, J. M., Caldwell, D. A., Barclay, T., Bryson, S. T., et al. (2013). *Kepler Data Release 21 Notes (KSCI-19061-001)*. Kepler mission
- [71] Torrence, C. and Compo, G. P. (1998). A Practical Guide to Wavelet Analysis. *Bulletin of the American Meteorological Society* 79, 61–78. doi:10.1175/1520-0477(1998)079
- [72] Woodard, M. F. and Noyes, R. W. (1985). Change of solar oscillation eigenfrequencies with the solar cycle. *Nature* 318, 449–450. doi:10.1038/318449a0
- [73] Yu, J., Huber, D., Bedding, T. R., Stello, D., Hon, M., Murphy, S. J., et al. (2018). Asteroseismology of 16,000 Kepler Red Giants: Global Oscillation Parameters, Masses, and Radii. *ApJS* 236, 42. doi:10.3847/1538-4365/aaaf74
- [74] Ziegler, C., Law, N. M., Baranec, C., Riddle, R., Duev, D. A., Howard, W., et al. (2018). Robo-AO Kepler Survey. IV. The Effect of Nearby Stars on 3857 Planetary Candidate Systems. *AJ* 155, 161. doi:10.3847/1538-3881/aab042

FUNDING

This paper includes data collected by the *Kepler* mission. Funding for the *Kepler* mission is provided by the NASA Science Mission directorate. Some of the data presented in this paper were obtained from the Mikulski Archive for Space Telescopes (MAST). STScI is operated by the Association of Universities for Research in Astronomy, Inc., under NASA contract NAS5-26555. Partly Based on observations obtained with the HERMES spectrograph on the Mercator Telescope, which is supported by the Research Foundation - Flanders (FWO), Belgium, the Research Council of KU Leuven, Belgium, the Fonds National de la Recherche Scientifique (F.R.S.-FNRS), Belgium, the Royal Observatory of Belgium, the Observatoire de Genève, Switzerland and the Thüringer Landessternwarte Tautenburg, Germany. S.M. acknowledges support by the National Aeronautics and Space Administration under Grant NNX15AF13G, by the National

Science Foundation grant AST-1411685 and the Ramon y Cajal fellowship number RYC-2015-17697. R.A.G. acknowledges the support from PLATO and GOLF CNES grants. ARGUS acknowledges the support from National Aeronautics and Space Administration under Grant NNX17AF27G. P.G.B. acknowledges the support of the MINECO under the fellowship program 'Juan de la Cierva incorporacion' (IJCI-2015-26034).

TABLES

Table 1. Non-oscillating stars with reliable rotation periods measured in this work. Surface gravity and effective temperatures come from the DR25 Stellar properties catalog (Mathur et al. 2017). Metallicity comes from the *Kepler* star properties DR25 (flag=0), APOGEE (flag=1), and from LAMOST (flag=2).

KIC	P_{rot} (days)	S_{ph} (ppm)	$\log g$	T_{eff} (K)	[Fe/H] (dex)	Flag
1164109	4.39 ± 0.47	501.62 ± 32.60	3.984	6608	-0.260	0
1434277	10.32 ± 0.75	5026.23 ± 201.58	4.499	5750	0.110	2
1576249	46.65 ± 5.69	113.81 ± 2.94	4.072	6195	-0.120	0
1718828	47.36 ± 2.89	193.56 ± 2.52	4.205	6372	-0.350	2
1724041	47.08 ± 6.46	92.38 ± 2.80	4.097	6711	-0.240	0
1724355	51.88 ± 10.09	112.89 ± 6.42	4.239	6127	-0.470	2
1864124	7.18 ± 0.56	141.04 ± 8.90	4.042	6337	-0.900	0
1868918	12.48 ± 1.03	44.49 ± 33.10	4.344	6054	0.038	1
2013883	59.09 ± 0.00	111.50 ± 2.61	4.058	6225	-0.026	1
2308753	2.77 ± 0.34	182.90 ± 9.77	4.150	6525	-0.020	2
2443534	10.86 ± 0.44	551.09 ± 22.96	4.487	6091	-0.140	0
2445004	13.52 ± 2.67	344.65 ± 13.21	4.169	6058	-0.180	0
2448426	13.31 ± 1.41	475.73 ± 18.09	4.223	6257	-0.420	0
2571934	5.47 ± 0.39	52.75 ± 5.40	4.167	6458	0.020	0
2578513	3.60 ± 0.22	116.55 ± 10.27	3.594	7201	-0.840	0
2580928	22.42 ± 1.50	226.53 ± 7.20	4.116	6052	-0.300	0
2709654	4.68 ± 0.45	52.55 ± 10.16	4.303	6642	-0.240	0
2718678	24.52 ± 1.97	235.31 ± 7.18	4.205	6095	-0.140	0
2722192	13.61 ± 1.06	3250.04 ± 114.00	4.482	5688	0.170	2
2837133	22.42 ± 1.80	3151.36 ± 86.29	4.334	5361	0.308	1

Table 2. KIC numbers of the non-oscillating stars without measured rotation periods.

KIC
1849587
2158850
2443543
2445385
2450979
2696938
2849969
2987466
2992960
2996629
3119256
3121024
3241299
3327769
3329136
3348288
3431597
3441637
3547874
3643799
3644869
3655608
3748392
3847825
4055330
4058963
4166365
4173599
4270083

FIGURE CAPTIONS

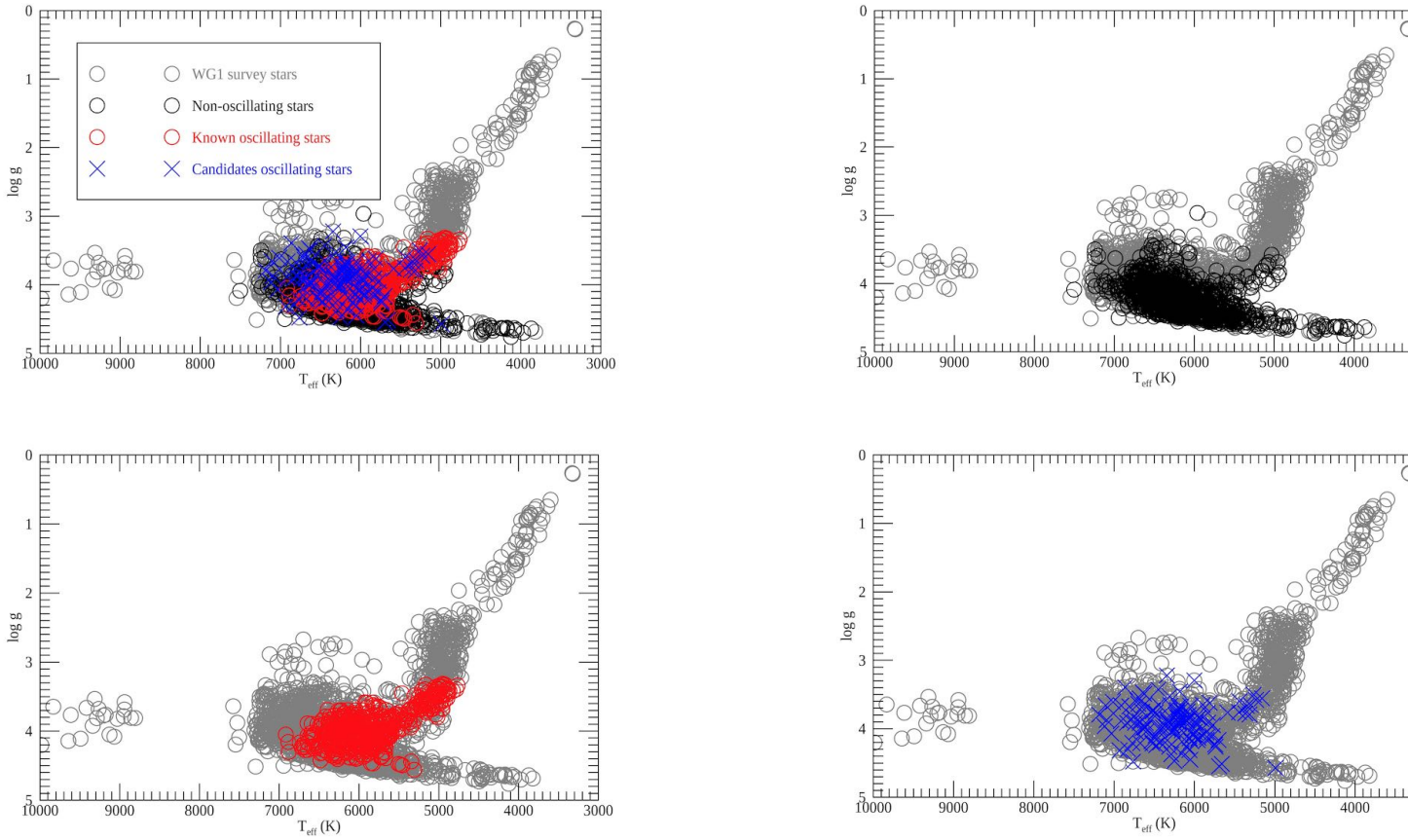


Figure 1. Hertzsprung-Russell Diagram for the different samples of stars mentioned in the paper. The grey circles represent KASC WG1 stars that were observed in short cadence during the survey phase. The red circles are the main-sequence stars with known oscillations from literature. The black circles correspond to the final set of 1,014 stars obtained as described in Section 2.2. The blue crosses are the new candidates with detection of oscillations.

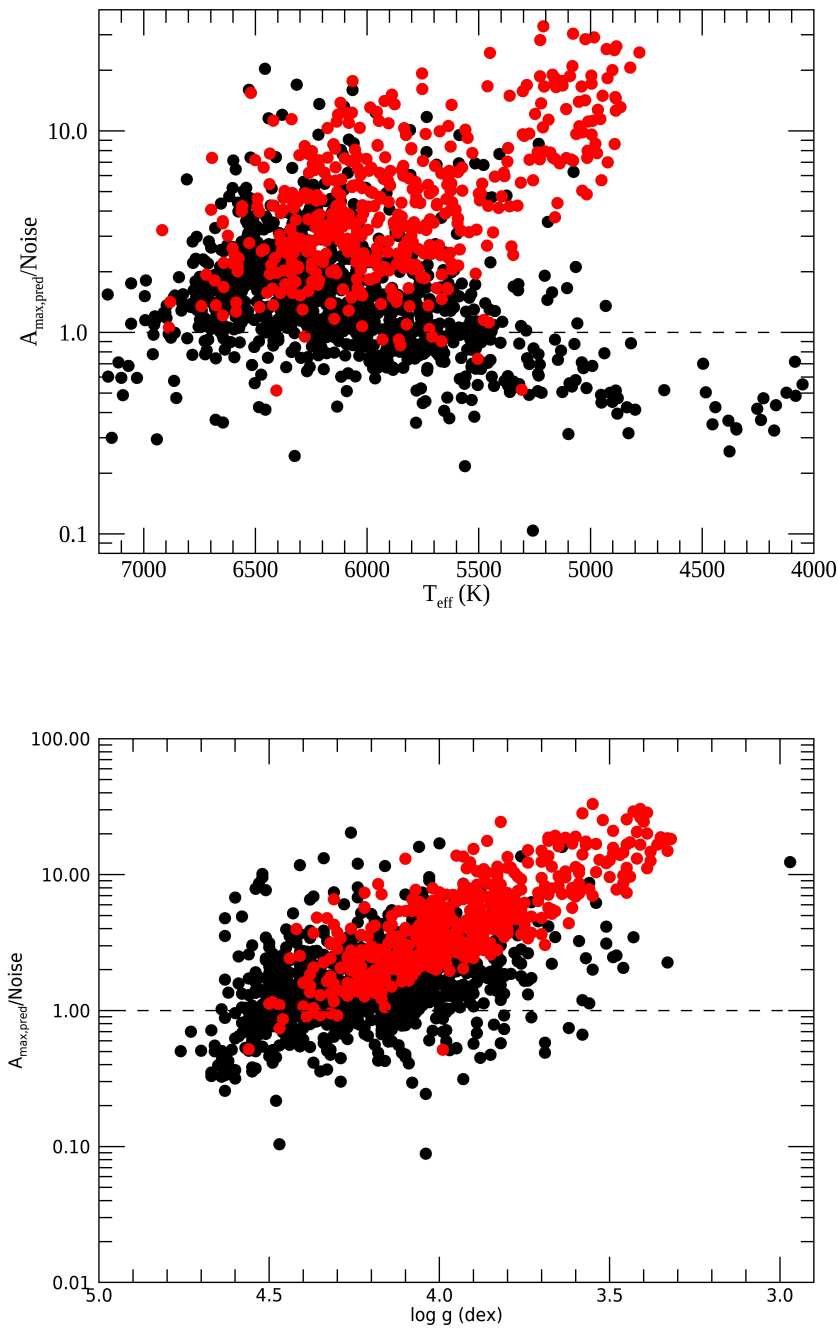


Figure 2. Ratio of the predicted maximum amplitude and the noise at high frequency as a function of the effective temperature (top panel) and as a function of surface gravity (bottom panel) for the stars without detected oscillations (black circles) and the stars with detected oscillations (red circles).

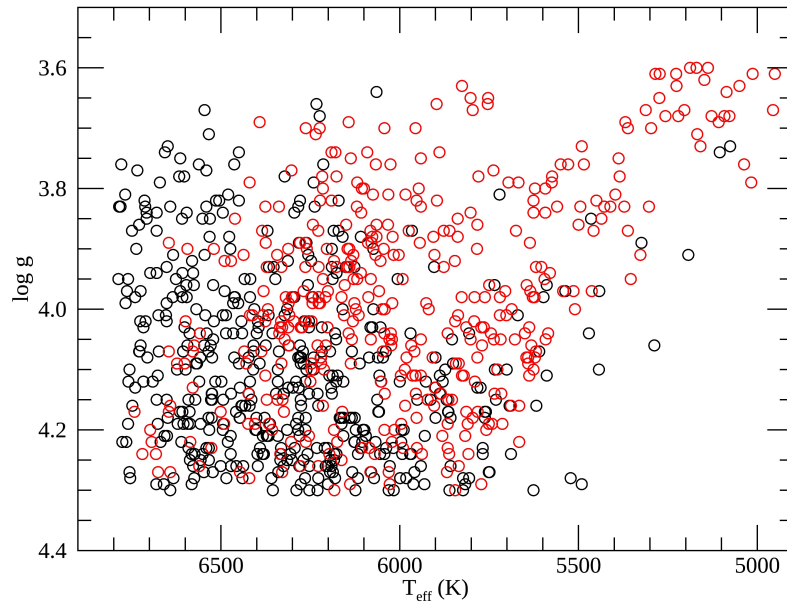


Figure 3. Hertzsprung-Russel Diagram for the stars selected as described in Section 2.3, with $A_{\max, \text{pred}}/\text{Noise} > 0.94$, $T_{\text{eff}} < 6,800$ K, and $\log g < 4.3$ dex. Stars without detected oscillations are represented with black circles and stars with detected oscillations in red circles.

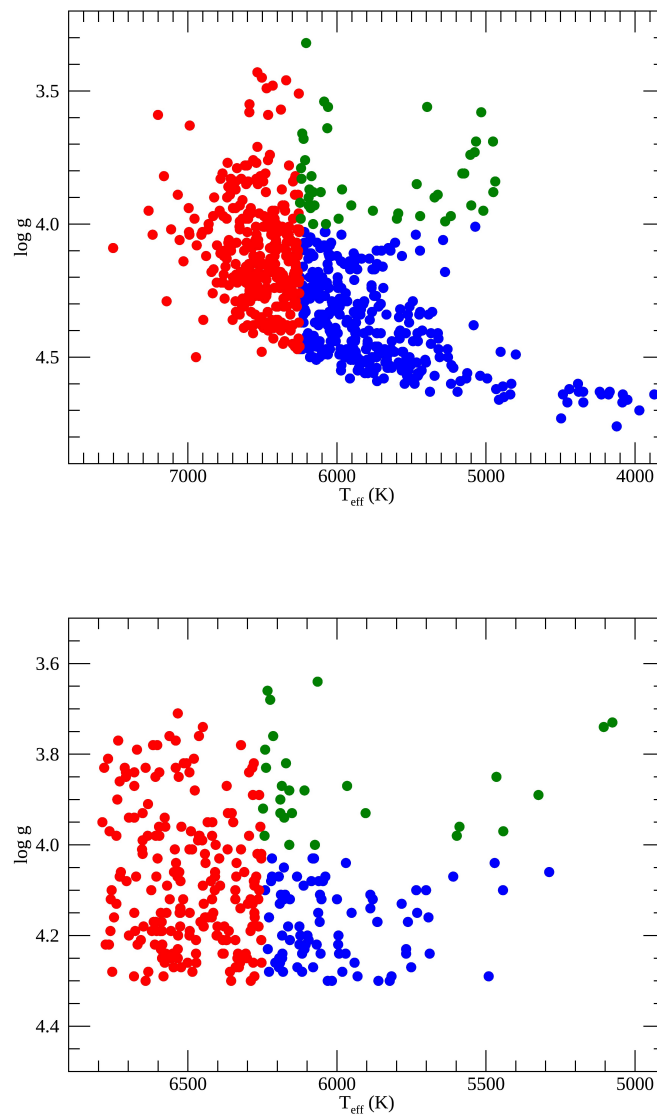


Figure 4. HR Diagram showing the hot dwarfs (red symbols), cool dwarfs (blue symbols), and subgiants (green symbols) as described in Section 4. Top panel: all the non oscillating stars with a measurement of rotation periods. Bottom panel: stars selected from the cut described in section 2.3 with a measurement of rotation period.

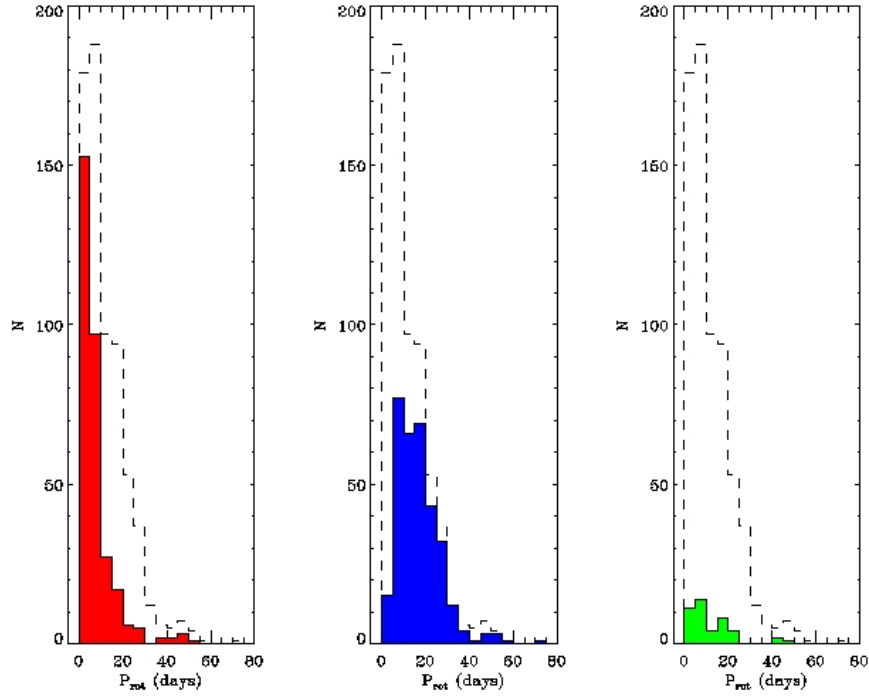


Figure 5. Distribution of the rotation periods for the full sample and the three categories of stars defined in Section 4: hot stars (left panel), cool dwarfs (middle panel), and subgiants (right panel). The black dash line in each panel represents the distribution for the full sample of stars with reliable rotation periods.

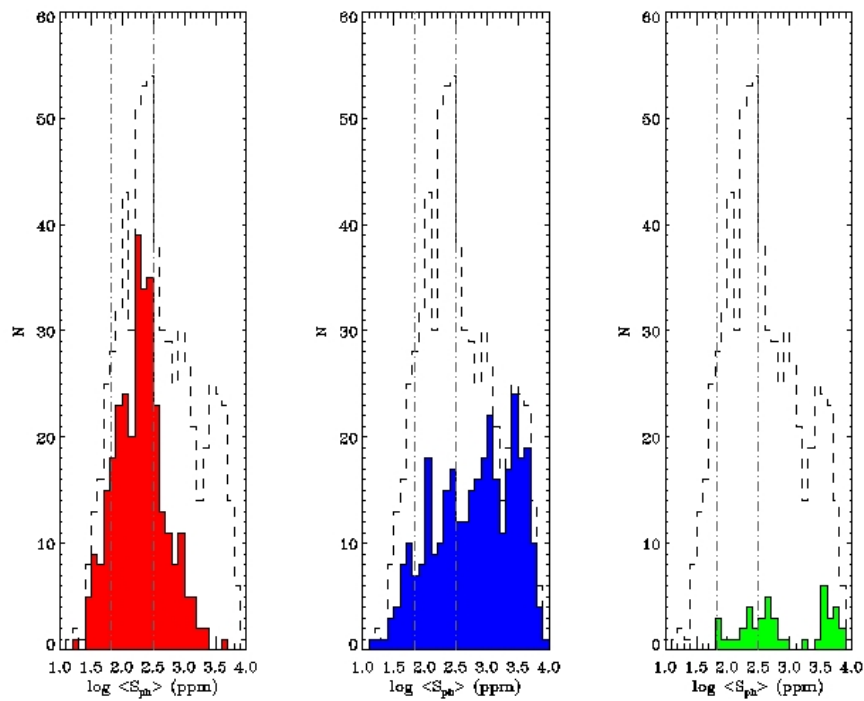


Figure 6. Distribution of the $\langle S_{ph} \rangle$ for the full sample and the three categories of stars as described in Section 4. Same legend as Figure 5. The grey dashed-dotted lines represent the values at minimum and maximum magnetic activity for the Sun.

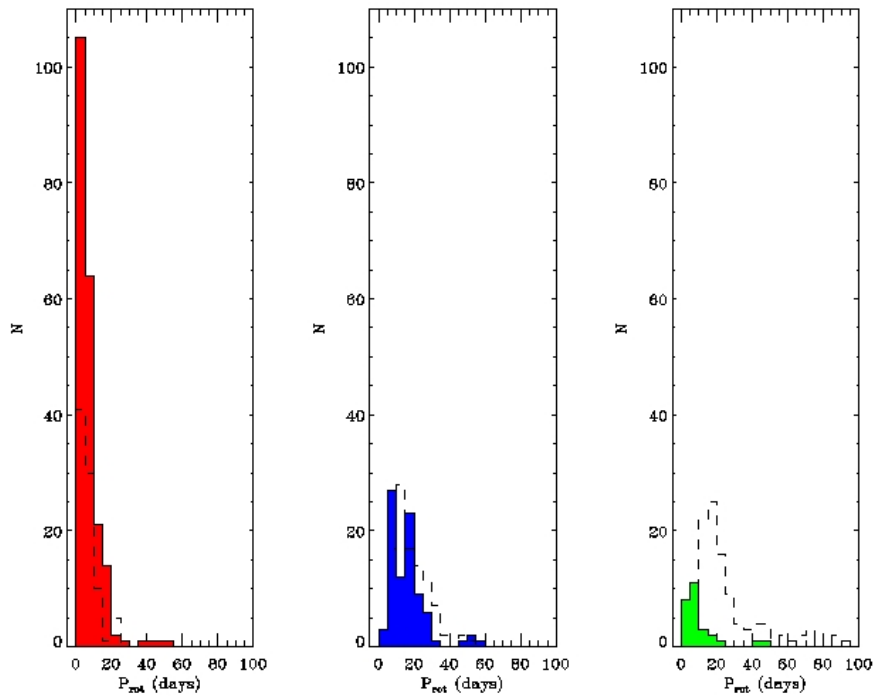


Figure 7. Rotation distribution for the non-oscillating stars selected as in bottom panel of Figure 4 with the same color code. The dash lines in each panel correspond to the rotation distribution of the oscillating stars in each spectral type.

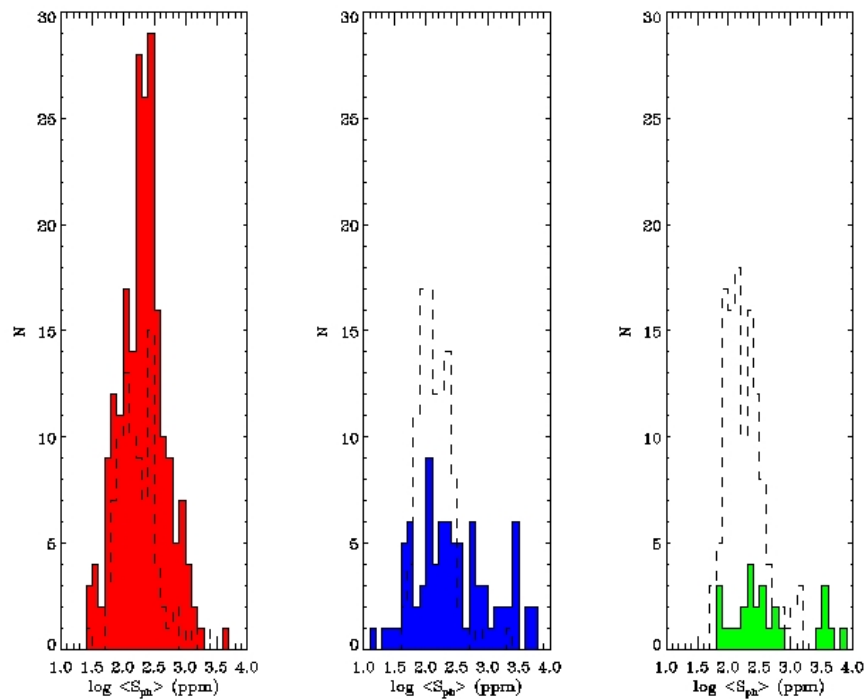


Figure 8. Distribution of the $\langle S_{ph} \rangle$ for the non-oscillating stars selected as in bottom panel of Figure 4 with the same color code. The dash lines in each panel correspond to the magnetic activity distribution of the oscillating stars in each spectral type.

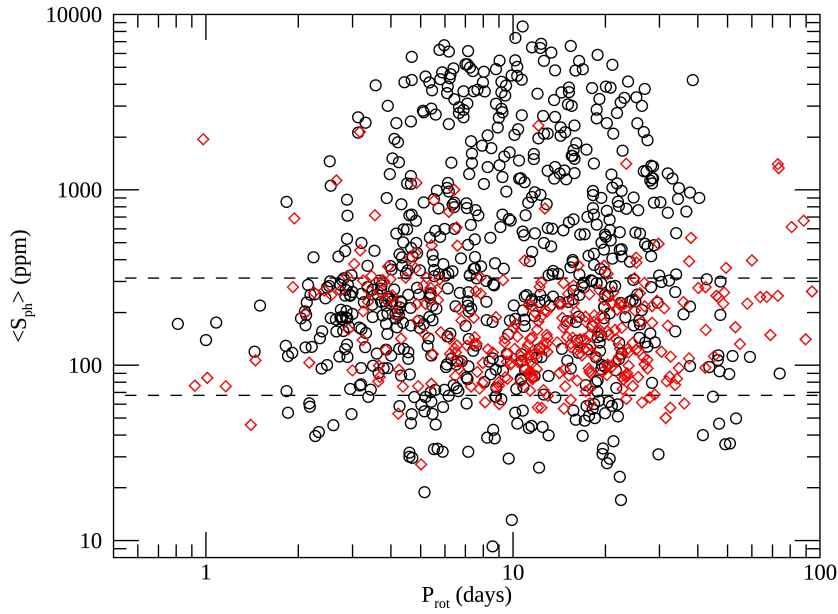


Figure 9. Proxy of the magnetic activity, $\langle S_{\text{ph}} \rangle$ as a function of the rotation period P_{rot} for the full sample. The black symbols represent the non-oscillating stars while the red symbols represent the stars with detected oscillations from García et al. (2014). The dash lines are the $\langle S_{\text{ph}} \rangle$ values at minimum and maximum activity of the Sun.

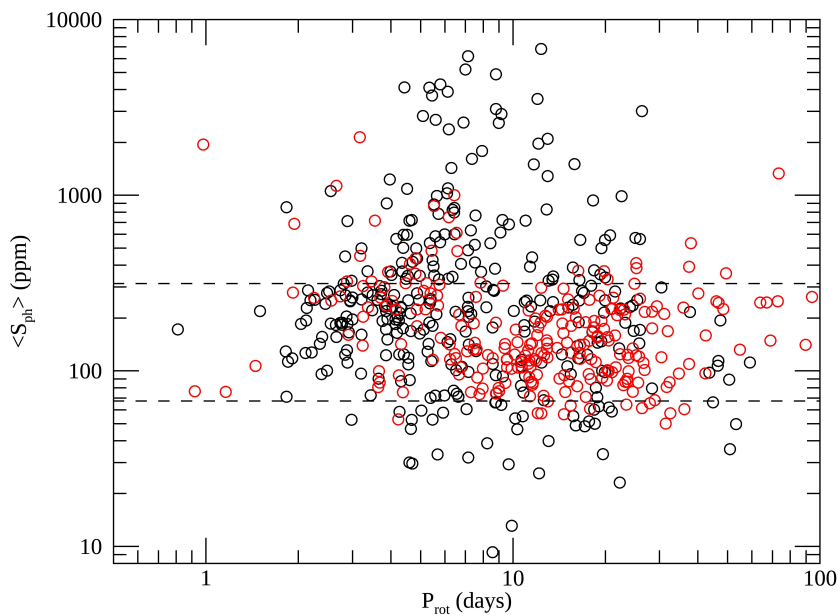


Figure 10. Same as Figure 9 but for stars selected as in Section 2.3.

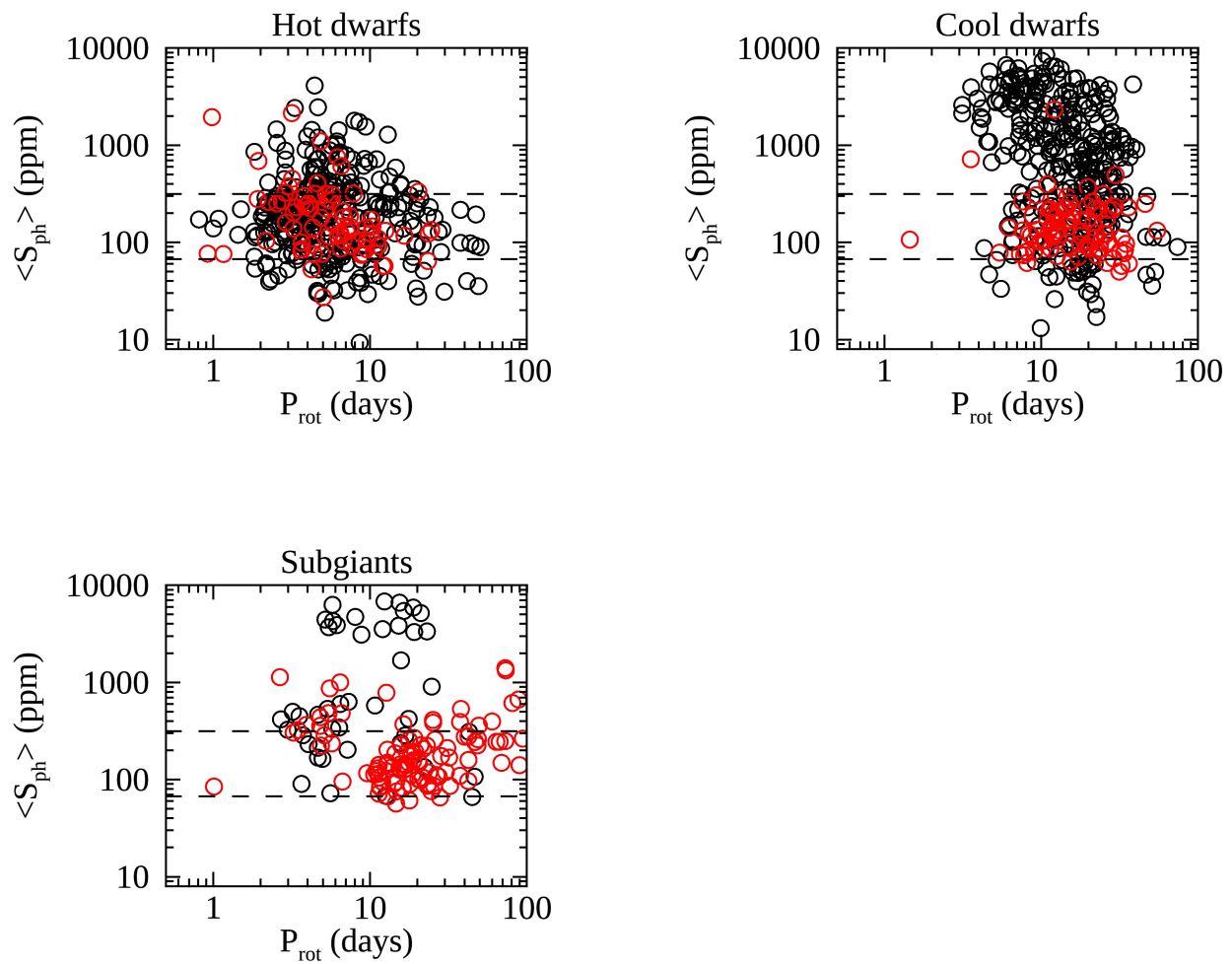


Figure 11. Same as Figure 9 but separated into the three categories of stars: hot dwarfs, cool dwarfs, and subgiants.

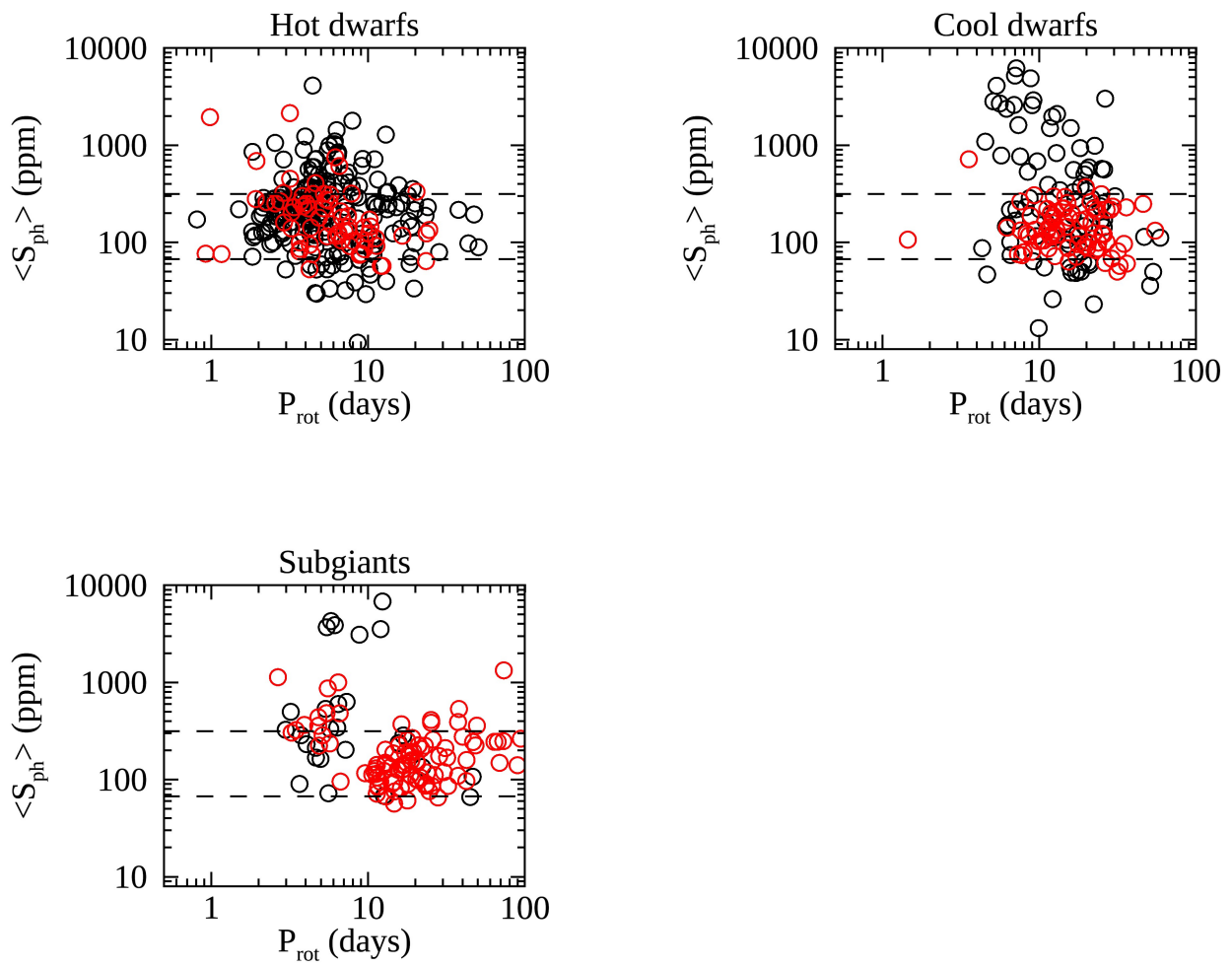


Figure 12. Same as Figure 10 but separated into the three categories of stars: hot dwarfs, cool dwarfs, and subgiants.

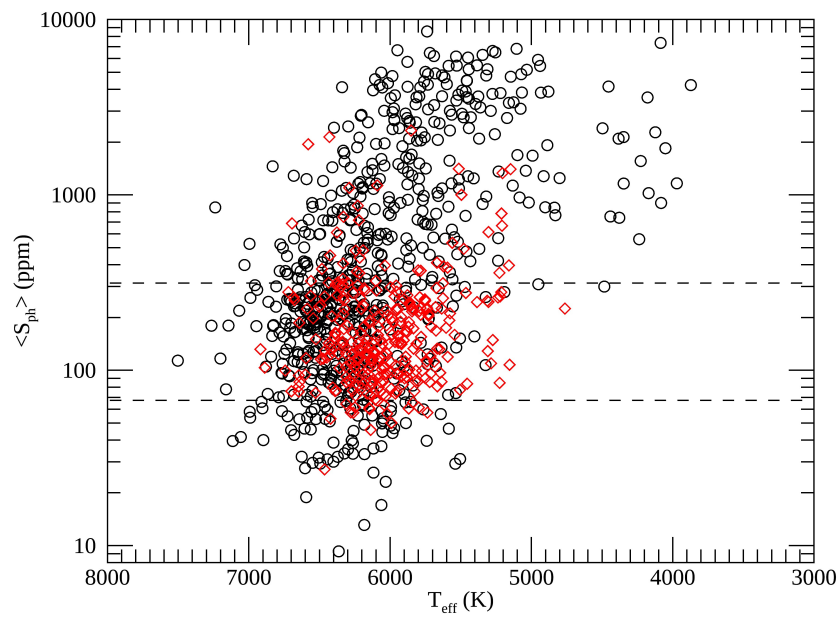


Figure 13. $\langle S_{ph} \rangle$ as a function of the effective temperature from the DR25 stellar properties catalog. Same legend as Figure 9.

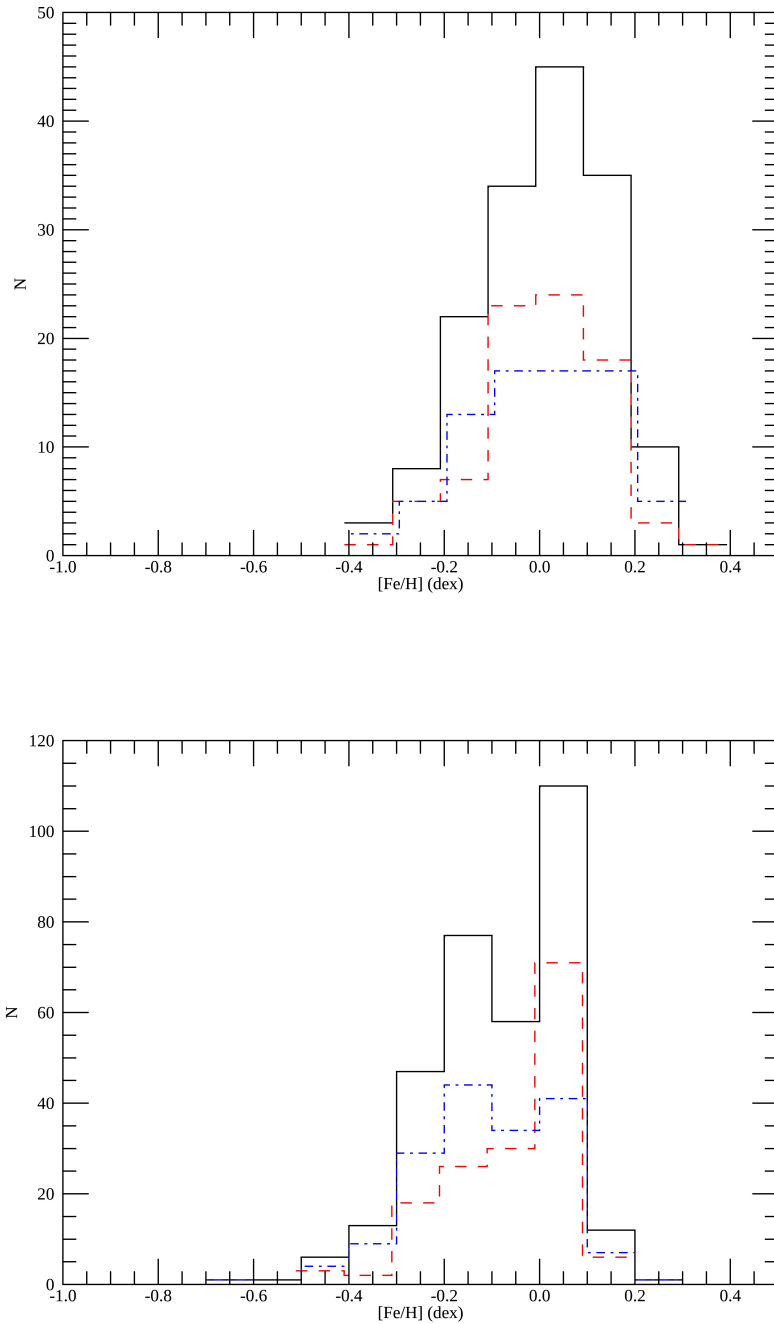


Figure 14. Histogram of metallicity for the non-oscillating stars using APOGEE DR14 for 158 stars (top) and LAMOST DR2 for 326 stars (bottom panel). The full sample in each panel is represented with the black solid line. Blue dot-dash line corresponds to the least active stars ($S_{\text{ph}} < S_{\text{ph},\odot,\text{max}}$) while red dash line corresponds to the most active stars ($S_{\text{ph}} > S_{\text{ph},\odot,\text{max}}$).

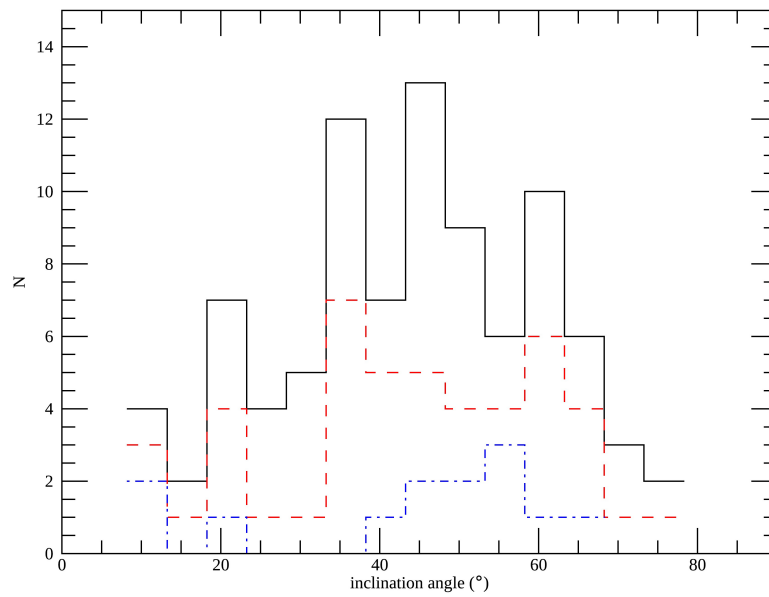


Figure 15. Distribution of inclination angles for stars with $v \sin i$ from APOGEE for stars with $A_{\text{max,pred}}/\text{Noise} > 0.94$. The red dash line represents the least active stars ($\langle S_{\text{ph}} \rangle < S_{\text{ph},\odot,\text{max}}$) while the blue dot-dash line represents the least active stars with a super-solar metallicity.